Editors' Suggestion | Featured in Physics

Decay Dynamics of a Single Spherical Domain in Near-Critical Phase-Separated Conditions

Raphael Saiseau,[1,2,*] Henri Truong,[1,3] Thomas Guérin,[1] Ulysse Delabre,[1] and Jean-Pierre Delville[1,†]
[1]University of Bordeaux, CNRS, LOMA, UMR 5798, F-33400, Talence, France
[2]Physics of Fluids, University of Twente, 7522 NB Enschede, The Netherlands
[3]University of Bordeaux, CNRS, CRPP, UMR 5031, F-33600, Pessac, France

(Received 8 February 2024; accepted 3 May 2024; published 3 July 2024)

Domain decay is at the heart of the so-called evaporation-condensation Ostwald-ripening regime of phase ordering kinetics, where the growth of large domains occurs at the expense of smaller ones, which are expected to "evaporate." We experimentally investigate such decay dynamics at the level of a single spherical domain picked from one phase in coexistence and brought into the other phase by an optomechanical approach, in a near-critical phase-separated binary liquid mixture. We observe that the decay dynamics is generally not compatible with the theoretically expected surface-tension decay laws for conserved order parameters. Using a mean-field description, we quantitatively explain this apparent disagreement by the gradient of solute concentrations induced by gravity close to a critical point. Finally, we determine the conditions for which buoyancy becomes negligible compared to capillarity and perform dedicated experiments that retrieve the predicted surface-tension induced decay exponent. The surface-tension driven decay dynamics of conserved order parameter systems in the presence and the absence of gravity, is thus established at the level of a single domain.

DOI: 10.1103/PhysRevLett.133.018201

Phase ordering kinetics is a ubiquitous and fundamental process [1,2], that characterizes the irreversible evolution of a system initially out-of-equilibrium into well separated coexisting phases. For conserved order parameter systems, the nucleated domains usually evolve from an intermediate free-growth regime to the so-called late stage Ostwald ripening [3–5], where the larger domains grow at the expense of the smaller ones which decay, or "evaporate" due to interfacial tension, as nicely demonstrated by the classical evaporation-condensation LSW theory of Lifshitz, Slyozov [6], and Wagner [7]. This very general phenomenon is at work in all phase transition dynamics involving conservation of the order parameter and has consequently huge implications in out-of-equilibrium liquids, soft matter, and material sciences [8–10].

The decay of the smallest domains was clearly observed in two-dimensional systems, such as metallic islands [11] or during a liquid-solid transition triggered in confined geometry [12] in order to illustrate the importance of correlations between evolving domains. In three dimensions, its investigation is essentially indirect as most coarsening experiments, performed at the scale of a large number of interacting droplets, and measured by scattering techniques [13] or by direct visualization of droplet assemblies [14,15], focus instead on the evolution of the droplet distribution and its comparison to LSW predictions. So, although at the basis of the evaporation-condensation Oswald ripening, the surface-tension driven evaporation of small droplets in conserved order parameter systems remains almost unexplored. Conversely, standard experiments [16,17] on the evaporation of single liquid drops report the classical R-squared law, in which the drop radius R evolves with time t as $R \sim (t_f - t)^{\alpha}$ with $\alpha = 1/2$, where t_f is the final evaporation time. The involved mechanism is nonetheless not driven by surface tension for scalar conserved systems, for which theory [2] predicts instead $\alpha = 1/3$ (unlike nonconserved systems, for which $\alpha = 1/2$ for surface-tension driven decay [2,18]). This exponent $\alpha = 1/3$ has been observed in the different context of the thinning dynamics of liquid necks [19,20]. However, surprisingly, this domain decay prediction at the scale of a single spherical drop has never been confronted to experiments, whereas it plays a key role in evaporation-condensation processes. This is the subject of the present Letter.

Starting from a near-critical phase-separated liquid mixture at equilibrium to keep the universality of Ising models, we use the optical radiation pressure of a laser wave to destabilize the meniscus separating the two phases in equilibrium and produce a size-controlled single drop of one phase immersed into the other, at a chosen altitude. Then, we turn off the laser and look at the drop evaporation. While we expected the $R \sim (t_f - t)^{1/3}$ scaling, our observations firmly indicate a richer dynamics due to gravity [21,22]. We build a dedicated mean-field model which incorporates gravity and confront our measurements to predictions. Finally, we "close the loop" by determining from the modeling the conditions for which buoyancy becomes

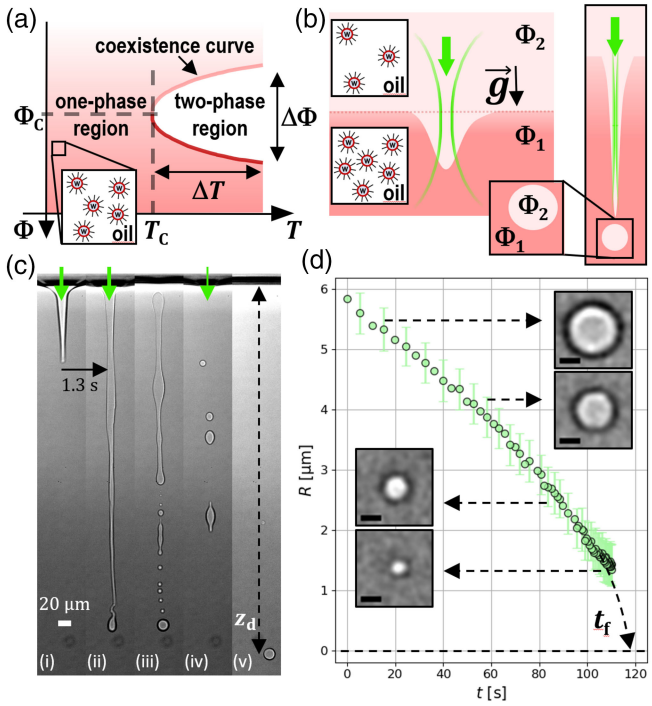

FIG. 1. (a) Schematic phase diagram of the critical micellar solution, with Φ the micellar volume fraction, and (T_c, Φ_c) the coordinates of the critical point. A cartoon of the water-in-oil micelles, of typical size 4 nm, is also shown (inset). (b) Schematics of the optical bending and jetting instability of the meniscus ($T > T_c$) induced by a laser beam focused at the meniscus (green). (c) Typical image sequence of the optical jetting instability. We show (i),(ii) the jet formation, (iii) the Rayleigh-Plateau instability when the laser is turned off the first time, (iv) the radiation pressure effect at lower laser power to force droplet coalescence, and (v) the resulting final evaporating droplet optically pushed to a given altitude. (d) Decay dynamics for $\Delta T = 4$ K, including snapshots, of the produced droplet when the laser is permanently turned off. t_f is the first time when the droplet cannot be detected any longer. Scale bars: 5 µm.

negligible compared to capillarity and performing dedicated experiments that retrieve the expected gravity-free decay exponent $\alpha = 1/3$. We thus characterize the surface-tension driven decay dynamics of conserved systems, at the level of a single spherical domain.

Experimental system.—We consider a water-in-oil micellar solution of critical composition (water, 9% wt, toluene, 70% wt, SDS, 4% wt, butanol, 17% wt) constituted of water nanodroplets coated by surfactant (the micelles, of radius $r \simeq 4$ nm) homogeneously dispersed in an oil continuum (the toluene) [23,24], see the Supplemental Material for details [25]. As a pseudobinary liquid mixture, where the micelles behave as the solute, it shows an Ising ($d = 3$, $n = 1$) low critical point at $T_C \simeq 38\,°\text{C}$, see Fig. 1(a). The microemulsion is contained inside a tight fused-quartz cell of 2 mm thickness thermally controlled with a PID in a homemade brass oven. When $\Delta T \equiv T - T_C > 0$, the solution separates into two phases of respective micellar volume fractions Φ_1 and Φ_2 (with $\Phi_2 < \Phi_1$), separated at equilibrium by an horizontal interface, called hereafter the meniscus. To produce thermodynamically metastable droplets, we use the optical radiation pressure of a continuous laser wave focused at the meniscus to induce a liquid jet [38,39] of the phase Φ_2 into the phase Φ_1, see Fig. 1(b). When the laser is turned off, drops are produced through the Rayleigh-Plateau instability [24]. Then, using again the radiation pressure at lower beam intensity, we force some of these drops to coalesce into a single one which is further pushed optomechanically to a chosen altitude, see Fig. 1(c). Thermodynamically out of equilibrium due to its finite size, the produced droplet immediately starts to evaporate while buoyancy makes it rise toward the meniscus.

The droplet decay is captured using ×20 or ×50 long working distance Olympus® microscope objectives and a Phantom® VEO340L camera. A custom-made ImageJ® code is used to detect the intensity gradient maxima at the drop edges to extract the droplet radius R, and we checked the calibration with other detection methods, see Supplemental Material [25]. The altitude z_d of the center of mass of the droplet is also recorded, with the convention that z_d increases in the downward direction, and $z_d = 0$ at the meniscus. An example of droplet evaporation dynamics is shown on Fig. 1(d).

On Fig. 2(a), we present several examples of individual droplet dynamics $R(t)$ for $\Delta T = 4$ K. While conservation of the order parameter predicts a regime $R(t) \propto (t_f - t)^{1/3}$, these measurements clearly demonstrate that this scaling is not verified. Instead, experimental data show a regime $R(t) \propto (t_f - t)^{\alpha}$, with $\alpha \simeq 0.5$–0.6. This behavior is confirmed down to $\Delta T = 0.2$ K [Fig. 2(b)]. As the decay amplitude varies from drop to drop (Fig. 2) and is correlated to the mean altitude $\langle z_d \rangle$ [defined as the temporal average of the spanned $z_d(t)$], a natural candidate for an additional physical effect impacting the evaporation could be gravity. Indeed, gravity is well known to affect the statics [40] and dynamics [2,21] of phase transitions. We thus develop a theoretical framework to understand the impact of gravity and surface tension on the evaporation dynamics of single droplets.

Theory.—We consider the free-energy functional

$$\mathcal{H}[\phi] = \int d\mathbf{x} \left\{ V(\phi) + \frac{\kappa}{2} (\nabla\phi)^2 - \rho_e g z \phi \right\}, \qquad (1)$$

where the order parameter ϕ is the local micellar volume fraction, $V(\phi)$ is a double-well potential, and κ gives the energy cost of local gradients of ϕ. Also, z is the vertical coordinate (increasing in the downward direction, with $z = 0$ at the meniscus), $\rho_e = \rho_{\text{micelle}} - \rho_{\text{solvent}}$ is the effective mass density of the micelles, and g is the earth gravitational acceleration. Next, we assume that the

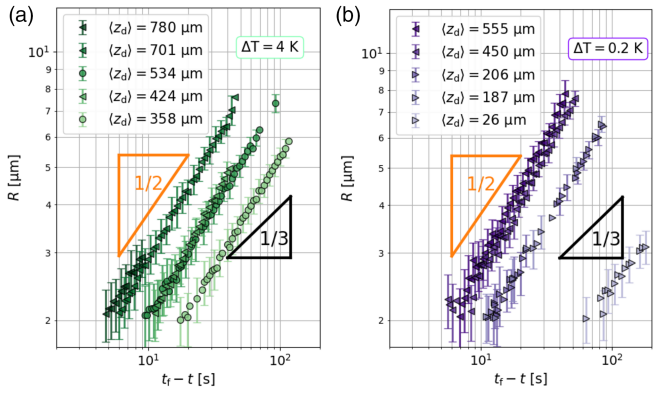

FIG. 2. Droplet radius R as a function of $t_f - t$ for (a) $\Delta T = 4$ and (b) $\Delta T = 0.2$ K. The legend indicates the average altitude $\langle z_d \rangle$.

dynamics satisfies the equations of the (noiseless) model H [41]:

$$\partial_t \phi + \mathbf{u} \cdot \nabla \phi = \lambda \nabla^2 \mu, \qquad \mu(\mathbf{x}) = \delta \mathcal{H}/\delta \phi(\mathbf{x}), \quad (2)$$

$$\eta \nabla^2 \mathbf{u} = \nabla p + \phi \nabla \mu, \qquad \nabla \cdot \mathbf{u} = 0, \quad (3)$$

with λ a kinetic coefficient, μ the chemical potential, η the viscosity and p the pressure. Here, the transport equation (2) for the conserved order parameter ϕ is coupled to Stokes' equation (3) describing the flow field $\mathbf{u}$ in the fluid (assumed to be incompressible) with an additional stress induced by chemical potential gradients. To ensure the conservation of the number of micelles, we impose that $\mathbf{u}$ and $\nabla \mu$ vanish at the boundaries of the system.

Sharp interface limit.—We consider the sharp-interface limit, in which κ is large enough so that, in each bulk phase i, the field ϕ is close to its equilibrium value ($\phi \simeq \Phi_i + \overline{\phi_i}$, with small $\overline{\phi_i}$), while ϕ varies sharply across interfaces. Here, Φ_1 and Φ_2 are the equilibrium values of ϕ on each side of the meniscus. In the sharp interface limit, following the arguments of Ref. [2] and adding gravity, an effective dynamics is obtained for $\overline{\phi}_i$ with effective boundary conditions at the interface [25]. In the bulk phases, at equilibrium, $\bar{\phi}_i \simeq \rho_e g z / V_i''$, where $V_i'' \equiv \partial_\phi^2 V|_{\Phi_i}$, so that, due to gravity, the concentration of micelles varies with the altitude z and differs from its standard value at coexistence equilibrium [42]. The dynamics for $\bar{\phi}$ obeys the advection diffusion equation

$$\partial_t \bar{\phi}_i + \mathbf{u} \cdot \nabla \bar{\phi}_i = D_i \nabla^2 \bar{\phi}_i, \qquad D_i = \lambda V_i''. \quad (4)$$

Next, the boundary conditions at an interface read

$$\bar{\phi}_i = \frac{-\gamma C}{\Delta \Phi V_i''}, \quad [\Delta \Phi (\mathbf{v} - \mathbf{u}) - D_2 \nabla \bar{\phi}_2 + D_1 \nabla \bar{\phi}_1] \hat{\mathbf{n}} = 0, \quad (5)$$

where $\Delta \Phi = \Phi_1 - \Phi_2$, $\mathbf{v}$ is the interface velocity, $\hat{\mathbf{n}}$ is the unit vector normal to the interface (pointing towards phase 1) and C is the total interface curvature. The first equation in Eq. (5) is a form of Gibbs-Thomson relation, while the second one expresses the conservation of the number of micelles.

Further assuming that advective and instationary terms in Eq. (4) are negligible (so that $\nabla^2 \bar{\phi}_i \simeq 0$), these equations can be solved by requiring that the equilibrium solution should be recovered far from the droplet. This leads to

$$\dot{R} = \frac{-\lambda}{R \Delta \Phi} \left(\frac{2\gamma}{R \Delta \Phi} + z_d \rho_e g \right), \qquad \dot{z_d} = -\frac{4 \rho_e \Delta \Phi g R^2}{15 \eta}, \quad (6)$$

where $\dot{R} \equiv \partial_t R$. The latter equation corresponds to Hadamard's formula for the sedimentation velocity of a liquid drop. Equations (6) describe the coupling between the evaporation dynamics and gravity. Two effects are at work: (i) first, if the droplet is at an altitude z_d, its evaporation dynamics is accelerated due to the increased micelle concentration at this altitude, and second (ii) a droplet moves and experiences different micelle concentrations due to Hadamard's law.

According to Eq. (6), when $R \to 0$, $\dot{z}_d$ vanishes and the final stage of evaporation occurs at constant z_d. In this case, integrating the equation for $\dot{R}$ leads to

$$f\left(\frac{z_d R(t)}{L_c^2} \right) = \frac{\lambda \Delta \Phi (t_f - t) (\rho_e g z_d)^3}{\gamma^2}, \quad (7)$$

where $f(u) = [(u-4)u/2] + 4 \ln [(u+2)/2]$ and $L_c = \sqrt{\gamma/(\rho_e g \Delta \Phi)}$ is the gravitational capillary length. As limiting cases, we retrieve, for small radii, the law for surface-tension dominated decay

$$R(t) \simeq \left[\frac{6 \lambda \gamma}{(\Delta \Phi)^2} (t_f - t) \right]^{1/3}, \quad (8)$$

whereas when $R \gg L_c^2 / z_d$, one obtains the gravity-dominated regime

$$R(t) \simeq [a(t_f - t)]^{1/2}, \qquad a = 2 \frac{\lambda \rho_e g z_d}{\Delta \Phi}. \quad (9)$$

This behavior looks similar to the classical R-squared laws, but here evaporation is driven by the difference between ϕ at the drop altitude and its value at which phase coexistence is allowed.

Experimental evidence of gravity effects.—On Fig. 3(a), we show experimental curves R^2 as a function of time. These curves are compatible with a linear relation $R^2(t) = a(t_f - t)$. The mean slope a is then reported as a function of z_d on Fig. 3(b), over a large variation of $\Delta T = 0.2$–16 K. A linear dependence of a on z_d is obtained, as predicted in the gravity dominated regime, see Eq. (9). The experimental values of $a/\langle z_d \rangle$ are reported on Fig. 3(c) and show a weak temperature dependency.

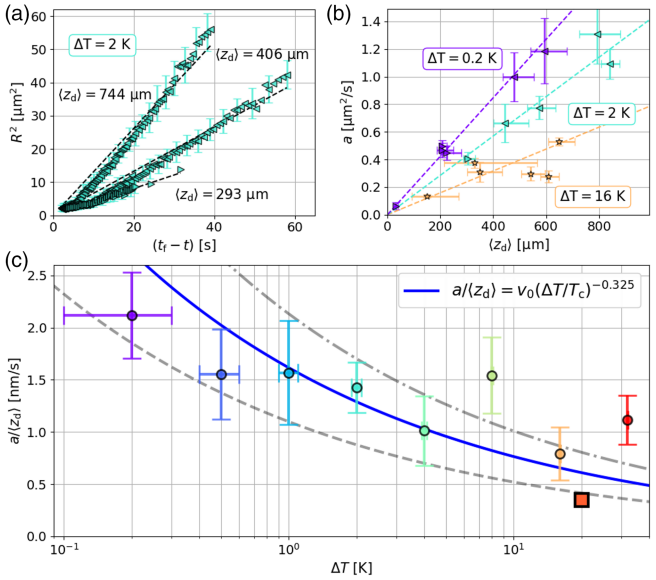

FIG. 3. (a) R^2 as a function of $t_f - t$ for different droplet mean altitude $\langle z_d \rangle$ for $\Delta T = 2$ K. Error bars are shown for one out of four data points for visibility issues. Dashed lines correspond to the linear fit $R^2 = a(t_f - t)$. (b) Fitted slope a as a function of $\langle z_d \rangle$, for $\Delta T = 0.2$, 2, and 16 K. The horizontal "error bars" indicate the range of z_d sampled during the evaporation, while vertical error bars show the standard deviation on a. Dashed lines are linear fits. (c) $a/\langle z_d \rangle$ as a function of ΔT. Blue continuous line: best fit with the law $a/\langle z_d \rangle = v_0(\Delta T/T_c)^{-0.325}$ with $v_0 = 0.25$ nm/s. Black dashed lines: same law with the coefficients $v_0 = 0.17, 0.33$ nm/s. Square symbol: $a/\langle z_d \rangle$ obtained from the theoretical analysis at $\Delta T = 20$ K (see text).

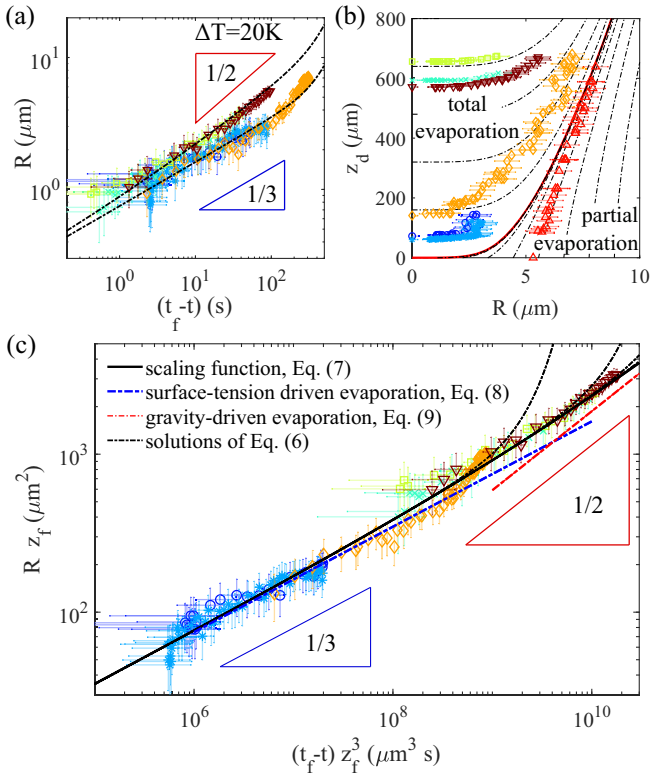

FIG. 4. Experimental and theoretical dynamics for $\Delta T = 20$ K. (a) R as a function of $t_f - t$, (b) same trajectories in the (R, z_d) plane and (c) $R(t)$ in rescaled coordinates, with $z_f \equiv z_d(t_f)$. Symbols: experimental values for six different drops, with an additional drop in (b) (red triangles). Dash-dotted black lines: solutions of Eq. (6). In (c), the continuous black line represents the scaling form (7), and dash-dotted blue and red lines indicate, respectively, the regimes with $\alpha = 1/3$ and $\alpha = 1/2$. Parameters of the theory: $L_c = 20$ μm, $\lambda\gamma/(\Delta\Phi)^2 = 0.07$ μm³/s, and $\rho_e \Delta\Phi g/\eta = 0.19$ μm^{-1} s^{-1} [25].

Theoretically, the diffusion coefficient $D_i = \lambda V_i''$ is usually believed to scale as $D_i \propto V_i''$, as demonstrated for spin exchange dynamics [43]. In our case, we conclude that λ does not depend on T near the critical point. Then, we expect $a/z_d \propto 1/\Delta\Phi \sim 1/(\Delta T)^\beta$ with $\beta \simeq 0.325$. Such scaling is compatible with the experiments, if one takes into account the dispersion of the data [Fig. 3(c)]. Thus, observations point towards gravity as being responsible for the acceleration of the evaporation dynamics from the expected exponent $\alpha = 1/3$ to the observed one $\alpha \simeq 1/2$.

Small drops near the meniscus: Surface-tension dominated dynamics.—Nonetheless, the model indicates that the decay exponent $\alpha = 1/3$ should be retrieved when $R \ll L_c^2/z_d$, i.e., when evaporating drops are small, close to the meniscus (where $z_d = 0$) and far from criticality (as L_c vanishes at the critical point). Since the gradient edge-detection method may be intrinsically limited for small radii [25], we conduct our measurement procedure as follows. Starting from calibrated silica beads of radii 1.15 and 2.18 μm in a water-glycerol mixture to reach refractive index contrasts close to those of our phase-separated system, a complementary image analysis method is developed, in agreement with the previously mentioned method [25]. On Fig. 4(a), we show the decay dynamics at $\Delta T = 20$ K, relatively far from the critical point. It is observed that some droplets decay with an exponent $\alpha = 1/3$, either over a large temporal window or only at the end of the dynamics, when $t \to t_f$. Figure 4(b) represents the trajectories of the same drops in the (R, z_d) plane, where one distinguishes between a region where drops reach the meniscus with a finite size, and a region where drops fully evaporate before reaching the meniscus, in agreement with the flow lines of the dynamical system (6). The comparison with Fig. 4(a) shows that the drops displaying $\alpha = 1/3$ during the longest time range are near the meniscus (small z_d, see, e.g., blue symbols), as expected theoretically. We also observe that $\alpha = 1/2$ appears when drops are far from the meniscus (large z_d, see, e.g., brown symbols). To quantify this effect, we rescale our data according to Eq. (7) on Fig. 4(c). The rescaled datasets fall onto a master curve, in agreement with the expression (7), with a fitted parameter a/z_d compatible with other experiments [square on Fig. 3(c)], with a capillary length $L_c = 20$ μm. While within the correct order of magnitude,

this value is 3–4 times smaller than expected. This underestimation could be attributed to the use of a simplified mean-field, isothermal, and quasistatic model, with an *a priori* assumed model H dynamics, which could describe real dynamics only at the cost of using renormalized coefficients. Nonetheless, even if refined theoretical ingredients may be needed, our model not only predicts the surface-tension ($\alpha = 1/3$) and the gravity-driven ($\alpha = 1/2$) evaporation regimes and their crossover, but also enables a full rescaling of the dataset and a semi-quantitative comparison with experiments, as shown in Fig. 4(c).

Conclusion.—With the aim of investigating the surface-tension driven decay at work in Ostwald-ripening mechanisms, we used an optomechanical strategy to produce the model situation of a single drop of one phase immersed into the other one. Our observations indicated a decay exponent $\alpha \simeq 1/2$, which was attributed to a gravity-induced concentration gradient. However, focusing on experimental conditions predicted by a theoretical analysis, we indeed measured the decay exponent $\alpha \simeq 1/3$ characteristic of surface-tension driven decay for conserved systems. Thus, even if the relative variation of concentration due to gravity is weak (see estimates in Supplemental Material [25]), it can still influence the domain decay, depending of the droplet size R, so that the decay exponent usually starts to be $1/2$ and may crossover to $1/3$ when R decreases enough due to evaporation. The smallness of the concentration gradient is a necessary condition to get the exponent $1/3$ but not sufficient. Consequently, our work raises experimentally and theoretically new insights on the decay component of the evaporation-condensation mechanism, so important in material sciences.

The authors thank the machine and electronic shops of LOMA for their technical contributions. The authors acknowledge financial support from the x through the projects FISICS ANR-15-CE30-0015-01 and ComplexEncounters ANR-21-CE30-0020. We thank Antoine Aubret for providing calibration beads, Quentin Moreno and Benjamin Sapaly for preliminary experiments, and Justine Roux and Gary Croise for their help in control experiments.

*r.a.saiseau@utwente.nl
†jean-pierre.delville@u-bordeaux.fr

[1] A. Onuki, *Phase Transition Dynamics* (Cambridge University Press, Cambridge, England, 2002).
[2] A. J. Bray, Theory of phase-ordering kinetics, Adv. Phys. **43**, 357 (1994).
[3] J. Marqusee and J. Ross, Kinetics of phase transitions: Theory of ostwald ripening, J. Chem. Phys. **79**, 373 (1983).
[4] P. Taylor, Ostwald ripening in emulsions, Adv. Colloid Interface Sci. **75**, 107 (1998).
[5] L. Ratke and P. W. Voorhees, *Growth and Coarsening: Ostwald Ripening in Material Processing* (Springer Science and Business Media, New York, 2002).
[6] I. M. Lifshitz and V. V. Slyozov, The kinetics of precipitation from supersaturated solid solutions, J. Phys. Chem. Solids **19**, 35 (1961).
[7] C. Wagner, Ostwald ripening theory, Ber. Bunsenges. Phys. Chem **65**, 581 (1961).
[8] D. Alloyeau, G. Prévot, Y. Le Bouar, T. Oikawa, C. Langlois, A. Loiseau, and C. Ricolleau, Ostwald ripening in nanoalloys: When thermodynamics drives a size-dependent particle composition, Phys. Rev. Lett. **105**, 255901 (2010).
[9] J. Jiao and D. J. Burgess, Ostwald ripening of water-in-hydrocarbon emulsions, J. Colloid Interface Sci. **264**, 509 (2003).
[10] A. J. Ardell and V. Ozolins, Trans-interface diffusion-controlled coarsening, Nat. Mater. **4**, 309 (2005).
[11] K. Morgenstern, E. Laegsgaard, and F. Besenbacher, Decay of two-dimensional islands on Ag(110), in *Collective Diffusion on Surfaces: Correlation Effects and Adatom Interactions: Proceedings of the NATO Advanced Research Workshop on Collective Diffusion on Surfaces: Correlation Effects and Adatom Interactions Prague, Czech Republic 2000* (Springer, New York, 2001), pp. 201–212.
[12] O. Krichevsky and J. Stavans, Ostwald ripening in a two-dimensional system: Correlation effects, Phys. Rev. E **52**, 1818 (1995).
[13] A. Cumming, P. Wiltzius, F. S. Bates, and J. H. Rosedale, Light-scattering experiments on phase-separation dynamics in binary fluid mixtures, Phys. Rev. A **45**, 885 (1992).
[14] V. Snyder, J. Alkemper, and P. Voorhees, Transient Ostwald ripening and the disagreement between steady-state coarsening theory and experiment, Acta Mater. **49**, 699 (2001).
[15] J. Alkemper, V. Snyder, N. Akaiwa, and P. Voorhees, Dynamics of late-stage phase separation: A test of theory, Phys. Rev. Lett. **82**, 2725 (1999).
[16] N. A. Fuchs, *Evaporation and Droplet Growth in Gaseous Media* (Pergamon Press, New York, 1959).
[17] A. Frohn and N. Roth, *Dynamics of Droplets* (Springer Science and Business Media, New York, 2000).
[18] P. L. Krapivsky, S. Redner, and E. Ben-Naim, *A Kinetic View of Statistical Physics* (Cambridge University Press, Cambridge, England, 2010).
[19] H. Y. Lo, Y. Liu, S. Y. Mak, Z. Xu, Y. Chao, K. J. Li, H. C. Shum, and L. Xu, Diffusion-dominated pinch-off of ultra-low surface tension fluids, Phys. Rev. Lett. **123**, 134501 (2019).
[20] L. K. Aagesen, A. E. Johnson, J. L. Fife, P. W. Voorhees, M. J. Miksis, S. O. Poulsen, E. M. Lauridsen, F. Marone, and M. Stampanoni, Universality and self-similarity in pinch-off of rods by bulk diffusion, Nat. Phys. **6**, 796 (2010).
[21] L. Ratke and W. Thieringer, The influence of particle motion on Ostwald ripening in liquids, Acta Metall. **33**, 1793 (1985).
[22] V. Kumaran, Effect of convective transport on droplet spinodal decomposition in fluids, J. Chem. Phys. **109**, 2437 (1998).

[23] R. Saiseau, C. Pedersen, A. Benjana, A. Carlson, U. Delabre, T. Salez, and J.-P. Delville, Near-critical spreading of droplets, Nat. Commun. **13**, 7442 (2022).
[24] J. Petit, D. Rivière, H. Kellay, and J.-P. Delville, Break-up dynamics of fluctuating liquid threads, Proc. Natl. Acad. Sci. U.S.A. **109**, 18327 (2012).
[25] See Supplemental Material at http://link.aps.org/supplemental/10.1103/PhysRevLett.133.018201, which presents the near-critical properties of the binary liquid used, the technical details for the edge detection of interfaces and its calibration using droplet relaxation dynamics, errors bars derivation, and details on the theoretical analysis, which includes Refs. [26–37].
[26] R. Wunenburger, B. Issenmann, E. Brasselet, C. Loussert, V. Hourtane, and J.-P. Delville, Fluid flows driven by light scattering, J. Fluid Mech. **666**, 273 (2011).
[27] R. Wunenburger, A. Casner, and J.-P. Delville, Light-induced deformation and instability of a liquid interface. II. Dynamics, Phys. Rev. E **73**, 036315 (2006).
[28] A. van der Bos, M.-J. van der Meulen, T. Driessen, M. van den Berg, H. Reinten, H. Wijshoff, M. Versluis, and D. Lohse, Velocity profile inside piezoacoustic inkjet droplets in flight: Comparison between experiment and numerical simulation, Phys. Rev. Appl. **1**, 014004 (2014).
[29] G. P. Bertollini, L. M. Oberdier, and Y. H. Lee, Image processing system to analyze droplet distributions in sprays, Opt. Eng. (N.Y.) **24**, 464 (1985).
[30] R. Barer and S. Joseph, Refractometry of living cells: Part I. Basic principles, J. Cell Sci. **S3-95**, 399 (1954).
[31] D. S. Dean, Langevin equation for the density of a system of interacting Langevin processes, J. Phys. A **29**, L613 (1996).
[32] S. Puri, N. Parekh, and S. Dattagupta, Phase ordering dynamics in a gravitational field, J. Stat. Phys. **75**, 839 (1994).
[33] C. Yeung, T. Rogers, A. Hernandez-Machado, and D. Jasnow, Phase separation dynamics in driven diffusive systems, J. Stat. Phys. **66**, 1071 (1992).
[34] J. Happel and H. Brenner, *Low Reynolds Number Hydrodynamics: With Special Applications to Particulate Media* (Springer Science and Business Media, New York, 1983).
[35] J. Lowengrub and L. Truskinovsky, Quasi-incompressible Cahn-Hilliard fluids and topological transitions, Proc. R. Soc. A **454**, 2617 (1998).
[36] L. D. Landau, *Fluid Mechanics*, 2nd ed. (Pergamon Press, New York, 1987).
[37] F. Hicks, T. C. Van Vechten, and C. Franck, Thermally perturbed barodiffusion in a binary liquid mixture, Phys. Rev. E **55**, 4158 (1997).
[38] A. Girot, J. Petit, R. Saiseau, T. Guérin, H. Chraibi, U. Delabre, and J. P. Delville, Conical interfaces between two immiscible fluids induced by an optical laser beam, Phys. Rev. Lett. **122**, 174501 (2019).
[39] A. Casner and J.-P. Delville, Laser-induced hydrodynamic instability of fluid interfaces, Phys. Rev. Lett. **90**, 144503 (2003).
[40] M. R. Moldover, J. V. Sengers, R. W. Gammon, and J. W. Hocken, Gravity effects in fluids near the gas-liquid critical point, Rev. Mod. Phys. **51**, 79 (1979).
[41] P. C. Hohenberg and B. I. Halperin, Theory of dynamic critical phenomena, Rev. Mod. Phys. **49**, 435 (1977).
[42] M. Giglio and A. Vendramini, Optical measurements of gravitationally induced concentration gradients near a liquid-liquid critical point, Phys. Rev. Lett. **35**, 168 (1975).
[43] K. Kawasaki, Diffusion constants near the critical point for time-dependent Ising models. I, Phys. Rev. **145**, 224 (1966).